Ferromagnetic transition and phase diagram of the one-dimensional Hubbard model with next-nearest-neighbor hopping

S. Daul and R. M. Noack
Institut de Physique Théorique, Université de Fribourg, CH-1700 Fribourg, Switzerland

We study the phase diagram of the one-dimensional Hubbard model with next-nearest-neighbor hopping using exact diagonalization, the density-matrix renormalization group, the Edwards variational ansatz, and an adaptation of weak-coupling calculations on the two-chain Hubbard model. We find that a substantial region of the strong-coupling phase diagram is ferromagnetic, and that three physically different limiting cases are connected in one ferromagnetic phase. At a point in the phase diagram at which there are two Fermi points at weak coupling, we study carefully the phase transition from the paramagnetic state to the fully polarized one as a function of the on-site Coulomb repulsion. We present evidence that the transition is second order and determine the critical exponents numerically. In this parameter regime, the system can be described as a Luttinger liquid at weak coupling. We extract the Luttinger-liquid parameters and show how their behavior differs from that of the nearest-neighbor Hubbard model. The general weak-coupling phase diagram can be mapped onto that of the two-chain Hubbard model. We exhibit explicitly the adapted phase diagram and determine its validity by numerically calculating spin and charge gaps using the density-matrix renormalization group.

PACS Numbers: 71.10.Fd, 75.10.Lp and 75.40.Mg

I. INTRODUCTION

Unlike strongly correlated phenomena such as antiferromagnetism or superconductivity which can be treated starting from a weak-coupling point of view, metallic ferromagnetism is an intrinsically intermediate or strong coupling phenomenon. Because of this, the origin of metallic ferromagnetism is still poorly understood, even after decades of research. The simplest model of correlated electrons, the Hubbard model, was introduced simultaneously by Gutzwiller,[1] Hubbard[2] and Kanamori[3] in 1963 in order to study ferromagnetism. Indeed, at a mean-field level, the Hubbard model seems to be a good starting point for ferromagnetism, because the Stoner criterion predicts a ferromagnetic ground state for a wide range of parameters. However, the inclusion of correlation effects makes the conditions for the appearance of ferromagnetism much more restrictive.[2]

There is one limit of the Hubbard model in which a ferromagnetic state can be obtained within an exact treatment. For $U = \infty$ the ground state of the half-filled system has macroscopic degeneracy since all states with different spin S have the same energy. For bipartite lattices (such as the hypercubic and bcc lattices) in dimension $d \geq 2$, and for fcc and hcp lattices with negative hopping integrals, Nagaoka[4] proved that when one hole is then added to the L-site system, the ground state of the model has maximum spin. It has not yet been proven possible to generalize Nagaoka's proof for the stability of ferromagnetism to a finite density of holes $\delta = 1 - n > 0$, making the treatment of the thermodynamic limit problematic. One can, however, use the opposite approach and try to show that the ferromagnetic state is unstable by applying a suitable variational wave function. Starting from the fully polarized state, one can flip a spin in an appropriate manner and then see if the corresponding energy is lower than the ferromagnetic one. If a lower energy can be found, the fully polarized ferromagnetic state is proven to be unstable. Recently, by choosing a highly sophisticated variational state, Wurth and co-workers[5] were able to bring the critical hole density δ_c above which the Nagaoka state is unstable at $U = \infty$ down to $\delta_c = 0.251$ for a square lattice. Exact diagonalization[6] and DMRG[7] studies suggest that δ_c could be even lower. Hence it cannot be ruled out that $\delta_c = 0$ for bipartite lattices, as is the case for the hyper-cubic lattice in infinite dimensions.[8] In contrast, for non-bipartite lattices, a partly polarized ground state (ferrimagnetism) has been obtained by Lieb.[9]

For one-dimensional systems, the situation is even less favorable for ferromagnetism. Lieb and Mattis[10] have proven that the ground state is unmagnetized for any real and particle-symmetric but otherwise arbitrary interaction. This theorem applies to a single band in $d = 1$, provided that the hopping is only between nearest neighbors and the interaction involves only densities. Since both conditions are fulfilled in the Hubbard model, its ground state in $d = 1$ cannot be ferromagnetic.

In principle, the Hubbard model is obtained from an extreme truncation of a more general Hamiltonian describing interacting electrons in a solid. Only the on-site interaction and one relevant band are kept. Nearest-neighbor interaction (e.g. direct exchange), band degeneracy and the associated Hund's rule couplings are totally neglected. In addition, the non-interacting band structure and density of states can be strongly affected by the lattice structure. In order to enhance the possibility of ferromagnetism, one can modify the simple Hubbard model by putting some of these neglected features back in.

Strack and Vollhardt[11] have studied a Hubbard model to which they have added all possible nearest-neighbor interactions: the usual interaction between charge (V), the density-dependent hopping (X), the Heisenberg exchange (F) and pair hopping (F'). They show that for a particular range of parameter values the model has maximum total spin at half-filling. These arguments can also be extended to the Nagaoka case of one hole.[12]

Another option is to take a multi-band Hamiltonian with d-band degeneracy together with a Hund's rule coupling between the different d orbitals. Okabe[13] has investigated the stability of the ferromagnetic state of such a model variationally, while Fleck and coworkers have studied a similar model including next-nearest-neighbor hopping.[14] These authors claim that the Hund's rule coupling is necessary to obtain ferromagnetism. Very recently, Bünemman and coworkers[15] have studied a two-band Hubbard model with a multi-band Gutzwiller wave function. They found that a ferromagnetic transition occurs at large interaction and stress that a finite value of the exchange interaction is also required. We will see here that ferromagnetism can be obtained in a non-orbitally-degenerate model.

Mielke[16] has proven the following theorem, equivalent to Hund's rule, for a Hubbard model with a flat band. If the model has an M-fold degenerate single-particle ground state, then for any number of electrons $N \leq M$ the fully polarized state (with total spin $S = \frac{N}{2}$) is a ground state of the system. Additional conditions that determine whether this ground state is unique are also given. This theorem has also been extended to nearly flat bands.[17] Recently, Tasaki[18] has considered a two-band Hubbard model with next-nearest-neighbor hopping. He has proven that the quarter–filled system (average electron density $n = 0.5$) is ferromagnetic for large enough on-site interaction U. Penc and coworkers[19] have extended this result to other fillings by studying a Hamiltonian in which a chemical potential is added to all even sites of the lattice to make a perturbative argument valid. We shall see below that this term is unnecessary to obtain a ferromagnetic ground state.

Several authors have studied the ordinary Hubbard model on various lattice structures. Ulmke[20] investigated the case of an fcc lattice using dynamical mean-field theory and quantum Monte Carlo simulations. He found ferromagnetism for intermediate values of U, using the density of states of the infinite-dimensional system. For the three-dimensional density of states he found that one must add next-nearest-neighbor hopping in order to obtain ferromagnetism. His general conclusion is that a necessary condition for ferromagnetism is a density of states with large spectral weight near the lower band edge. Hanisch and coworkers[21] have investigated the stability of saturated ferromagnetism using a variational approach for various lattice structures in two and three dimensions. Their conclusions are similar to the previous ones, namely that a particle-hole asymmetry and a divergent density of states at the lower band energy are necessary ingredients for obtaining a ferromagnetic ground state. Similar conclusions have been reached very recently using the spectral density approach[22] and dynamical mean-field theory with the Non-Crossing Approximation.[23]

In the small density limit, the ferromagnetic state of the Hubbard model with arbitrary non-diagonal hopping and with a band structure with a quadratic dispersion about the band minima has been shown to be unstable for $d > 3$, while for $d = 2$ a small window of parameters for which the fully polarized state is not destabilized still remains.[24] Indeed, a projector quantum Monte Carlo calculation[25] yields ferromagnetism precisely in this allowed region for the two-dimensional Hubbard model on a square lattice with next-nearest-neighbor hopping. Finally, a renormalization group calculation for this model[26] also yields ferromagnetism in a particular regime.

In this work,[27] we study perhaps the simplest case of a Hubbard model exhibiting ferromagnetism: the one-dimensional Hubbard model with an additional next-nearest-neighbor hopping. Previously, exact diagonalization,[24] variational[28] and Density-Matrix Renormalization Group (DMRG) calculations[29] on this model have already concluded that there is an extensive ferromagnetic phase for large enough coupling U. A weak-coupling analysis[30] applied to this one-dimensional model leads to a phase with a spin gap which is the one-dimensional analog of a superconductor. Projector QMC and DMRG calculations for the special case of half-filling[31] have recently been carried out at weak to intermediate coupling and are consistent with the weak-coupling analysis. Here we treat the strong and weak-coupling phase diagrams of the model comprehensively with numerical and variational techniques, and link them by studying the phase transition using exact diagonalization and DMRG calculations.

This paper is organized as follows. In Sec. II, we discuss the basic properties of the model, motivate the existence of ferromagnetism by discussing calculations on three and four site clusters, and discuss exactly treatable limiting cases at interaction $U = \infty$, some of which yield ferromagnetic ground states. The results of a variational calculation of the $U = \infty$ phase diagram using the Edwards variational ansatz are presented in Sec. III. While this technique was previously applied to this model in Ref. 28 at finite U, here we discuss the $U = \infty$ phase diagram and include a determination of the total spin of the variational state. Exact diagonalization calculations, presented in Sec. IV, are used to illustrate the determination of the critical interaction strength U_c at the ferromagnetic transition, to determine the order of the phase transition, and to examine the scaling of U_c for small next-nearest-neighbor hopping t_2. In Sec. V we use the DMRG to determine U_c as a function of density for three different t_2 regimes, discuss the behavior of the Luttinger liquid parameters at the transition from a Luttinger liquid regime to the ferromagnetic regime, and discuss the behavior of the spin-spin correlation function

near the transition. We present a determination of the strong-coupling ($U = \infty$) and weak-coupling phase diagrams in Sec. VI. The strong-coupling phase diagram is calculated using the DMRG, and the weak-coupling phase diagram is determined by adapting the results of Balents and Fisher[32] for the two-chain Hubbard model to this model, as suggested by Fabrizio.[30] A DMRG calculation of the spin and charge gaps at weak but finite U is then used to check the validity of the weak-coupling phase diagram. The DMRG calculations of U_c and the $U = \infty$ phase diagram were reported in a preliminary form in Ref. 29, but here they are carried out with more accuracy and the discussion is extended.

II. THE $t_1 - t_2$ CHAIN

A. The model

We consider the one-dimensional Hubbard model with next-nearest-neighbor hopping (see Fig. 1) with the Hamiltonian

$$H = -t_1 \sum_{i,\sigma} \left(c^\dagger_{i+1\sigma} c_{i\sigma} + h.c. \right) - t_2 \sum_{i,\sigma} \left(c^\dagger_{i+2\sigma} c_{i\sigma} + h.c. \right) + U \sum_i n_{i\uparrow} n_{i\downarrow}. \quad (1)$$

We will call this model the $t_1 - t_2$ chain.

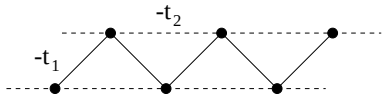

FIG. 1. The $t_1 - t_2$ chain.

The summation is over all L sites and spin σ. Here we will always take U positive and set $\hbar = 1$. The sign of t_1 is arbitrary since a gauge transformation $c_j \to e^{i\pi j} c_j$ can reverse it, so we set $t_1 = 1$ without loss of generality, and measure all energies in units of t_1. This Hamiltonian conserves the number of particles, the total spin $\mathbf{S}$ and its projection onto the quantization axis, S_z. If a particle-hole transformation is applied to the system, the transformation $t_2 \to -t_2$ is necessary to recover the original Hamiltonian. Therefore, the parameter regime $n > 1$, $t_2 > 0$ maps to $n < 1$, $t_2 < 0$ and the regime $n > 1$, $t_2 < 0$ maps to $n < 1$, $t_2 > 0$ (see Fig. 2). Because a definite order of the particles is no longer enforced when $t_2 \neq 0$, the Lieb-Mattis theorem[10] does not apply and, indeed, we will see that we do find ferromagnetism.

The effect of the sign of t_2 can be understood by considering the Hamiltonian of Eq. (1) with $L = 3$, $N = 2$ particles, and open boundary conditions. This three-site model, treated by Tasaki in Ref. 33, has a ferromagnetic ground state only when $t_2 < 0$. For this choice of sign, the triangular structure frustrates the antiferromagnetic order normally found in the Hubbard model.

For $U = 0$ and periodic boundary conditions H can be diagonalized by Fourier transformation yielding

$$H = \sum_{k,\sigma} \epsilon(k) c^\dagger_{k\sigma} c_{k\sigma} \quad (2)$$

with k an integer multiple of $\frac{2\pi}{L}$ and

$$\epsilon(k) = -2t_1 \cos k - 2t_2 \cos 2k. \quad (3)$$

The dispersion $\epsilon(k)$ will have one minimum at $k = 0$ for $t_2 > -0.25$ and two minima at finite k for $t_2 < -0.25$. Similarly, there will be maxima in $\epsilon(k)$ at $k = \pm\pi$ for $t_2 < 0.25$, but will shifted away from $k = \pi$ for $t_2 > 0.25$. Therefore, for small $|t_2|$, $\epsilon(k)$ does not differ qualitatively from the $t_2 = 0$ band structure, and there are two Fermi points for arbitrary electron density n. On the other hand, for $t_2 < -0.25$ and sufficiently small densities or for $t_2 > 0.25$ and sufficiently large densities, the Fermi surface has four Fermi points, namely $\pm k_{F_1}$ and $\pm k_{F_2}$ and, as we will see, can be mapped to a two-band model at weak coupling. The resulting $U = 0$ ground-state phase diagram is depicted in Fig. 2. Note that we take the horizontal axis to be $-t_2$ in this and all subsequent phase diagrams in order to better display the $t_2 < 0$, $n < 1$ region on which we will primarily concentrate in this work.

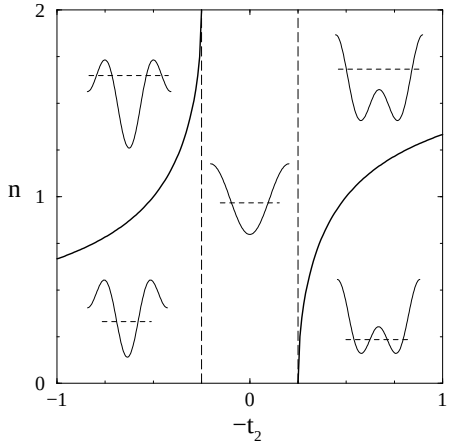

FIG. 2. $U = 0$ phase diagram. The inset plots show the qualitative behavior of $\epsilon(k)$ in the different regions with the Fermi level indicated by the dashed line.

B. Square cluster

It is useful to solve the Hamiltonian of Eq. (1) exactly for $L = 4$ and periodic boundary conditions in analogy with the solution of the three-site problem discussed above. This will allow us to further examine the effect of the sign of t_2 on the ground state, and also will illustrate finite-size effects due to open and closed shell configurations. As depicted in Fig. 3, one obtains the Hubbard model on a square with additional diagonal hopping.

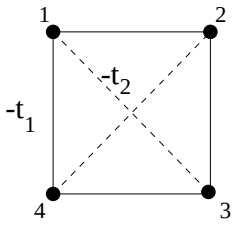

FIG. 3. Square cluster.

We consider the $U = \infty$ limit with $N = 2$ and $N = 3$ electrons and minimum S_z (e.g. $S_z = 0$ for $N = 2$). The dimension of the Hilbert space is 12 in both cases. With the aid of group theory, the problem can be solved analytically. The Hamiltonian has the symmetry of the group C_{4v} (see Table I), and can be diagonalized using the symmetry-adapted wave functions. The eigenvalues are labeled by the corresponding irreducible representations (A_1, A_2, B_1, B_2, E). In order to see whether a state is fully polarized or not, we check whether the eigenfunction is symmetric or antisymmetric. The irreducible representations A_1, B_1 and B_2 are symmetric and A_2 is antisymmetric.[34] Since the global wave function is required to be antisymmetric and the spin function of a fully polarized state is symmetric, the ferromagnetic state must belong to the representation A_2.

An analysis of the eigenvalues (see Tables II and III) leads to the following conclusions:
$N = 2$: For $t_2 > -0.5$ the ground state has $S = 0$. In this case the fully polarized state is not a closed shell state and it seems that for this reason it can not be the ground state. Similar open shell effects have also been observed in numerical exact diagonalization calculations for larger systems and other fillings.[28]

For $t_2 < -0.5$ (where the single-particle spectrum has two minima) the ferromagnetic ($S = 1$) ground state of representation A_2 is degenerate with the non-magnetic ($S = 0$) state of B_1. This is in agreement with Mielke's theorem,[16] according to which the ferromagnetic ground state is unique only when a restricted single-particle density matrix of the ferromagnetic ground state is irreducible, and degenerate when it is reducible. That the latter case applies for $L = 4$ can be confirmed by explicit calculation of this single-particle density matrix. It is interesting to note that for $N = 2$ on systems with $L > 4$, it can be shown numerically that the ground state is ferromagnetic and unique when the single-particle spectrum has two minima. This degeneracy therefore seems to be an artifact of the high symmetry of the $L = 4$ system.
$N = 3$: For any $t_2 < 0$ the ground state is ferromagnetic. This is actually the Nagaoka case of one hole in a half-filled band.

C. Special limits for $U = \infty$

For $U = \infty$ and negative t_2, ferromagnetism has analytically been shown to exist in three different limits. For one hole in a half-filled band, the Nagaoka mechanism leads to a ferromagnetic ground state;[35] for $|t_2| \to 0$, Sigrist and coworkers have shown that the model is ferromagnetic for all densities;[36] and for $|t_2| > 0.25$, where the band structure has two minima, Müller-Hartmann[37] has shown that the low-density limit is ferromagnetic. These three limits are indicated in the schematic phase diagram shown in Fig. 4. In addition, for $|t_2| \to \infty$ the model can be mapped onto two decoupled Hubbard chains, which cannot be ferromagnetic due to the Lieb–Mattis theorem.

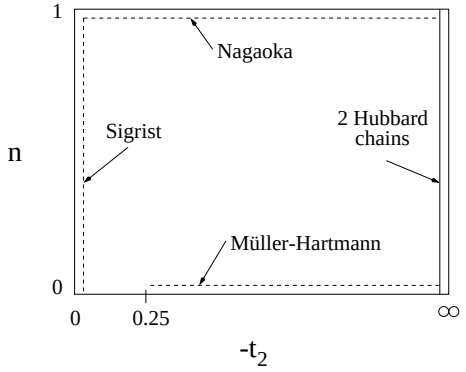

FIG. 4. Schematic $U = \infty$ phase diagram.

III. VARIATIONAL APPROACH

The fully polarized state

$$|F\rangle = \prod_{k<k_F} c^\dagger_{k\uparrow}|0\rangle \tag{4}$$

is an eigenstate of Hamiltonian (1) with energy

$$E_{\rm ferro} = \sum_{k<k_F} \epsilon_k, \tag{5}$$

where ϵ_k is the single-particle dispersion and k_F is the Fermi wave vector for the ferromagnetic state. The ferromagnetic state $|F\rangle$ is certainly unstable if a variational state with one flipped spin and a lower energy can be found. In order to put good constraints on the extent of a ferromagnetic phase, it is important to use as good a variational wave function as possible. A particularly sophisticated ansatz due to Edwards is defined by

$$|\chi\rangle = \frac{1}{\sqrt{L}} \sum_{\ell=1}^{L} e^{iq\ell} c^\dagger_{\ell\downarrow} \prod_{\alpha=1}^{N-1} c^\dagger_{\alpha\uparrow}(\ell)|0\rangle \tag{6}$$

where

$$c^\dagger_{\alpha\uparrow}(\ell) = \sum_{m=1}^{L} \varphi_\alpha(m-\ell) c^\dagger_{m\uparrow} \tag{7}$$

creates an up-spin electron in an orbital that is determined variationally. The variational parameters are the

wave vector q and the $(N-1)L$ amplitudes $\varphi_\alpha(\ell)$. For $t_2 = 0$ this variational wave function includes the Bethe Ansatz as a special case, and is therefore an exact solution of the simple Hubbard chain.[38] This ansatz has previously been applied to the $t_1 - t_2$ model in order to calculate critical U values in Ref. 28, but here we show the results of additional calculations, including the full $U = \infty$ phase diagram.

The variational energy for orthonormal one-particle orbitals reads[39]

$$\begin{aligned} &E(q, \{\varphi_\alpha(\ell)\}) = \\ &-2t_1 \cos(q)\ \det S^{(1)} - 2t_2 \cos(2q)\ \det S^{(2)} \\ &-2t_1\ \mathrm{tr} S^{(1)} -\ 2t_2\ \mathrm{tr} S^{(2)}\ +\ U \sum_{\alpha,\beta} \varphi^*_\alpha(0)\varphi_\beta(0) \end{aligned} \tag{8}$$

with overlap matrices $S^{(\delta)}_{\alpha\beta}$ defined as

$$S^{(\delta)}_{\alpha\beta} = \sum_{\ell=1}^{L} \varphi^*_\alpha(\ell)\varphi_\beta(\ell+\delta). \tag{9}$$

We use the conjugate gradient method[40] to minimize the energy. The derivatives

$$\frac{\partial E}{\partial \varphi_\alpha(\ell)} \tag{10}$$

can be calculated analytically and are given in Appendix A. After each iteration the orbitals are orthonormalized using the modified Gram-Schmidt method. The initial orbitals, which must be chosen so that they are close enough to the final wave functions $\varphi_\alpha(\ell)$, are taken to be the $N-1$ lowest eigenfunctions of the Hamiltonian (1) with $U = 0$ and a site impurity at 0. Care has to be taken in choosing the particle number N. In particular, the corresponding non-interacting ground state must be non-degenerate (closed shell) in order to obtain well-behaved convergence of the conjugate gradient calculation.

Here we want to determine the $U = \infty$ phase diagram. Since there is no double occupancy when $U = \infty$, $\varphi_\alpha(0) = 0$ for all α and the energy gradient with respect to $\varphi_\alpha(0)$ can be excluded. We also calculate the total spin $\mathbf{S} = \sum_i \mathbf{S}_i$ of the wave function. Using the commutator $[S^+, S^-] = 2S_z$ and working at a particular S_z, we obtain

$$\langle \mathbf{S}^2 \rangle = \frac{N}{2}\left(\frac{N}{2} - 1\right) + \langle S^- S^+ \rangle. \tag{11}$$

By applying Wick's theorem to the down spin operators, we can write

$$\langle S^- S^+ \rangle = \frac{1}{L} \sum_{\ell,m} e^{iq(\ell-m)} \langle 0| \prod_\alpha b_\alpha(\ell)\ c_{\ell\uparrow} c^\dagger_{m\uparrow}\ \prod_\beta b^+_\beta(m)|0\rangle. \tag{12}$$

The elements of the sum can be expressed in term of a determinant [cf. Eq. (A12) in Ref. 39; care must be taken since there are typographical errors], leading to

$$\begin{aligned} \langle S^- S^+ \rangle = 1 - \sum_{\delta=1}^{L-1} &\cos(q\delta) \det S^{(\delta)} \\ &\left[\sum_{\alpha,\beta} \varphi_\alpha(\delta) {S^{(\delta)}_{\alpha\beta}}^{-1} \varphi_\alpha(L-\delta) \right]. \end{aligned} \tag{13}$$

For $S = S_{\max} = N/2$, (11) implies $\langle S^- S^+ \rangle = N$, whereas for $S = S_{\max} - 1$, $\langle S^- S^+ \rangle$ must vanish. When the ferromagnetic state is destabilized, we find that $\langle S^- S^+ \rangle \approx 0.01 - 0.1$. That this expectation value is not an eigenvalue of S^2 is an indication that the variational wave function is not an eigenstate of H, as opposed to the $t_2 = 0$ case. The resulting $U = \infty$ phase diagram is displayed in Fig. 5. As one can see from the figure, all four of the analytically treatable limits of Sec. II C are, for the most part, reproduced, and the three ferromagnetic regions are connected to one another.

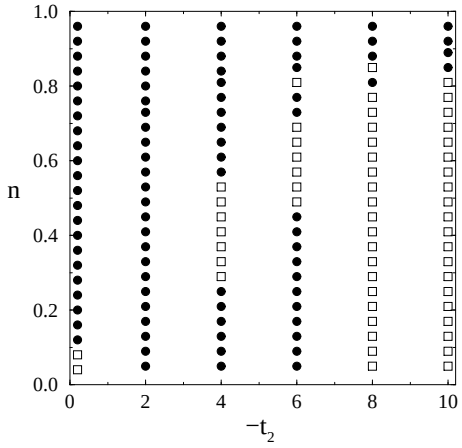

FIG. 5. $U = \infty$ phase diagram obtained with ansatz (6) from numerical calculations on an $L = 100$ lattice. The filled circles represent stable ferromagnetic states and the open squares unstable ones.

One anomaly is that for small $|t_2|$ the ferromagnetic state is destabilized at low density. As we will see, this does not occur in the DMRG calculations. This discrepancy is probably due to the large finite size effects on finite lattices at low densities that come from the difference between closed and open shells when the system has periodic boundary conditions. We have already seen this behavior for $L = 4$ in Sec. II B. The alternating paramagnetic and fully polarized states as a function of n near the upper boundary of the paramagnetic phase are another illustration of these finite-size effects. In addition, for small n and $|t_2| \geq 8$, the ferromagnetic state is unstable in a regime expected to be ferromagnetic by the Müller–Hartmann argument. However, this argument is valid in the limit of small n, and here the lowest obtainable n is limited by N/L.

IV. EXACT DIAGONALIZATION

We have performed numerical diagonalization using the Lanczos[41] and the Davidson[42] algorithms for chains of up to length $L = 16$, and various numbers of electrons N and boundary conditions. These methods permit us to obtain both the numerically exact energy and the wave function of the ground state on a finite cluster.

A. Boundary conditions

On small lattices, it is important to analyze carefully the effect of boundary conditions. In order to understand which boundary conditions should be used, we consider the case of $N = 2$ electrons on a $L = 12$ system with $t_2 = -0.1$. With periodic boundary conditions the system is never ferromagnetic, similar to the four-site model discussed in Sec. II B. In fact, this seems to be the case for all lattice sizes L. For anti-periodic boundary conditions, the single-particle spectrum has 2 degenerate minima at $k = \pm\frac{\pi}{12}$. Due to Mielke's theorem[16] the model is fully polarized for all $U > 0$. Therefore both boundary conditions are unable to reproduce the low-density regime with a paramagnetic ground state for small U and a ferromagnetic ground state for large U.

Only with open boundary conditions do we obtain a non-magnetic ground state for small U and a ferromagnetic one for large U. We find that the critical value occurs at $U_c \approx 11$. Therefore, in order to minimize the effect of the boundary conditions, we will take open boundary conditions for all exact diagonalization calculations as well as for the DMRG calculations described subsequently.

B. Determination of U_c

In order to determine the critical value of U above which the ferromagnetic state is the ground state, we start at small U, for which the ground state is not magnetic, and increase U until we reach the fully polarized state. The transition point can be determined by examining the behavior of the energy E_0.

As discussed in Sec. III, the energy of the fully polarized ferromagnetic state, $E_{\rm ferro}$, does not depend on U and is exactly known. Thus, if $E_0(U) = E_0(\tilde{U}) = E_{\rm ferro}$ for all $U > \tilde{U}$, we identify $\tilde{U}$ with U_c. This can be confirmed by verifying that the lowest eigenvalue is the same in all S_z-subspaces, since then the ground state must have a degeneracy of $2S_{\rm max}+1$, or by calculating the expectation value of the total spin operator in the ground state,

$$\langle\psi_0|\mathbf{S}^2|\psi_0\rangle = \sum_{i,j}\langle\psi_0|\mathbf{S}_i\mathbf{S}_j|\psi_0\rangle = S(S+1). \qquad (14)$$

For $U > U_c$ one will obtain $S = S_{\rm max}$. In Fig. 6 we clearly see that the values for U_c obtained using these two criteria are the same.

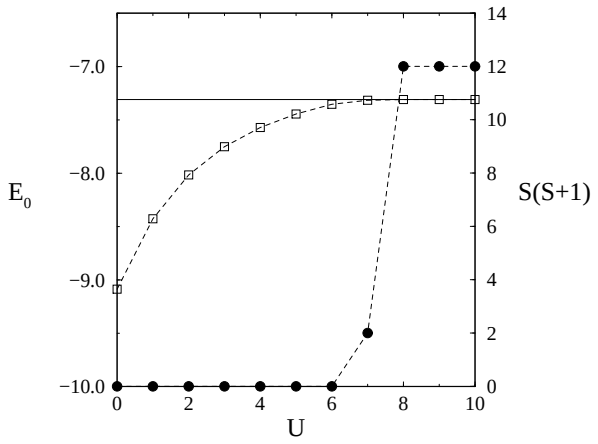

FIG. 6. E_0 (open squares) and $\langle\psi_0|\mathbf{S}^2|\psi_0\rangle = S(S+1)$ (filled circles) for a system of size $L = 12$ with $N = 6$ and $t_2 = -0.2$. The horizontal solid line is the energy of the fully polarized state.

C. Order of the transition

In order to determine the order of the transition, we investigate with very high precision the ground state energy $E_0(U)$ around U_c. Since there are many states with energy very close to E_0 a very large number of iterations are needed in the Davidson procedure in order to obtain convergence (more than 1000 $H|\psi\rangle$ multiplications).

If the transition is first order, the ground state will jump from $S = 0$ to $S = S_{\rm max}$ and $E_0(U)$ will have a kink at U_c. On the other hand, if the transition is second (or higher) order there will be no kink in the energy as a function of U and S will smoothly take on all values from 0 to $S_{\rm max}$. In the thermodynamic limit, a second order transition requires that

$$\lim_{U\to U_c^-}\frac{\partial E_0}{\partial U} = \lim_{U\to U_c^+}\frac{\partial E_0}{\partial U}, \qquad (15)$$

i.e. that the derivative of the ground state energy is continuous through the transition.

In order to further clarify this issue we can follow the lowest energy state with a particular spin S. Since utilizing the $\mathbf{S}^2$ quantum number in the exact diagonalization program is technically difficult to implement, we follow a state of a particular $\mathbf{S}^2$ by diagonalizing the augmented Hamiltonian

$$H' = H + \lambda\mathbf{S}^2 \qquad (16)$$

in different S_z-subspaces with $\lambda > 0$. For large enough λ, the lowest energy state within a given S_z sector will

have the minimum S value. In Fig. 7 we clearly see that the spin S of the ground state takes on all intermediate values as U is increased. This is an indication that Eq. (15) will be satisfied in the thermodynamic limit and that the transition is continuous. Here we have chosen the parameters $n = 0.5, t_2 = -0.2$ so that the system is in a regime with two Fermi points at $U = 0$. As will be shown in Sec. VI B, the system is a Luttinger liquid for weak U at these parameters. The transition is therefore from a Luttinger liquid to a ferromagnet. Further evidence that the transition is second order based on the behavior of the Luttinger-liquid parameters will be given in Sec. V.

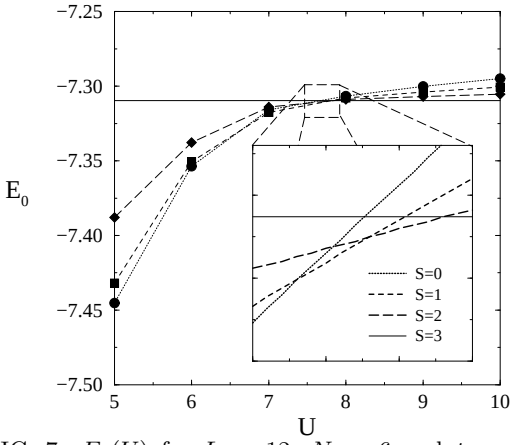

FIG. 7. $E_0(U)$ for $L = 12$, $N = 6$ and $t_2 = -0.2$ for $S = 0, 1, 2, 3$. The inset is a blowup of the indicated region.

D. Small t_2

We have already seen that for $t_2 = 0$ the fully polarized state always has a higher energy than the $S = 0$ state unless $U = \infty$. For large but finite U, we can treat the model perturbatively in $\frac{1}{U}$. For $t_2 = 0$ and $n = 1$ this yields the one-dimensional Heisenberg model. For the non-half-filled system and $|t_2| \ll t_1$, we obtain, to first order in $\frac{1}{U}$,

$$H = -t_1 \sum_{i,\sigma} \left(c^\dagger_{i+1\sigma} c_{i\sigma} + h.c. \right) + \left(J_{\rm eff} + \frac{4t_1^2}{U} \right) \sum_i \mathbf{S}_i \mathbf{S}_{i+1} - \frac{t_1^2}{U} \sum_{i,\sigma,\sigma'} \lambda_{\sigma\sigma'} c^\dagger_{i+2\sigma} c^\dagger_{i+1-\sigma} c_{i+1-\sigma'} c_{i\sigma'} + h.c.. \quad (17)$$

Here $\lambda_{\sigma\sigma} = +1$, $\lambda_{\sigma-\sigma} = -1$ and

$$J_{\rm eff} = \frac{t_2}{2\pi} \left[\frac{2}{\pi n} \sin^2 \pi n - \sin 2\pi n \right] \quad (18)$$

is obtained as in Ref. 36. If $\sigma = \sigma'$ the third term of Eq. (17) leads to a permutation of the spin part of the wave function. The resulting matrix element (proportional to $\frac{1}{U}$) can be incorporated into the second term to yield an effective Heisenberg coupling

$$\tilde{J} = J_{\rm eff} + \frac{\gamma}{U} \quad (19)$$

where γ depends only on the filling of the system and, in principle, can be calculated. Hence the coupling is ferromagnetic when

$$-t_2 > \frac{\gamma}{U} \quad (20)$$

and for small $|t_2|$ the critical U should behave as

$$U_c \sim |t_2|^{-1}. \quad (21)$$

A numerical evaluation of U_c in this low $|t_2|$ regime (shown in Fig. 8) obtained from exact diagonalization is reproduced quite well by this form.

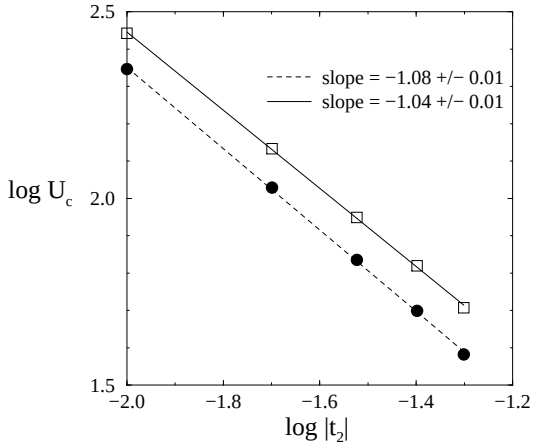

FIG. 8. U_c as a function of t_2 for $L = 10$ on a log-log scale. The filled circles are for $N = 4$ and the open squares for $N = 6$ while the solid and dashed lines are obtained using linear regression.

V. DENSITY MATRIX RENORMALIZATION GROUP

We now investigate much larger systems[29] by applying the powerful and already widely used Density-Matrix Renormalization Group technique.[43] The DMRG is a variational procedure which can be used to obtain the energies of the ground state and low-lying excited states very accurately, as well as to compute a wide variety of equal-time correlation functions. Here we use the finite-size algorithm for system sizes of up to $L = 140$ and keep up to 1000 states in the last iteration. The efficiency of the algorithm is improved by keeping track of the basis transformations in order to calculate a good initial guess for the wave function after adding a site to the system.[44] Calculations applied to the $t_1 - t_2$ model on small systems

show extremely good agreement with exact diagonalization results (up to 10 figures). The total discarded weight of the density-matrix eigenvalues provides an estimate of the truncation error. In the calculations performed here, the discarded density-matrix weight ranges from 10^{-8} to 10^{-6}. The estimated error in the DMRG results shown here, determined by examining the convergence with the number of states kept, is of the order of the plotting symbol size or less, unless explicitly discussed.

We have also included the possibility of adding a term $\lambda \mathbf{S}^2$ to the Hamiltonian. Turning on $\lambda > 0$ shifts states of higher total spin S to higher energies. This shift is known for a particular S since $\mathbf{S}^2$ commutes with the Hamiltonian. This addition is useful for two reasons. First, since the DMRG can only determine a limited number of excited states accurately for a given number of states kept, it allows more excited states to be accessed within a particular S subspace. Second, it allows one to follow states of a particular S individually, even if they are not the ground state of a particular S_z subspace for $\lambda = 0$. This trick is particularly useful near the ferromagnetic transition, where the ground state often has nonzero total spin, and states with different total spin are very close in energy. The numerical problem of the mixing of different total S states when they are near-degenerate in energy is also sometimes relieved when λ is turned on.

A. U_c as a function of the density

In order to determine U_c we investigate the behavior of the ground state energy and the expectation value of the total spin operator $\langle \mathbf{S}^2 \rangle$ of the ground state, as in the previously described exact diagonalization calculations (see Sec. IV B). Here we have chosen to carry out the calculations on an $L = 50$ lattice because the finite-size effects are negligible upon further increasing L. In Fig. 9 we show results for various values of t_2 as a function of the density n.

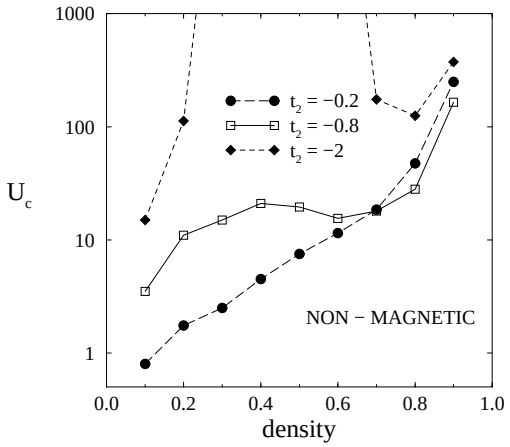

FIG. 9. U_c as a function of density for $L = 50$ on a log-linear scale for three different values of t_2.

The three curves show three different representative behaviors. In all cases, as $n \to 1$, U_c diverges to reach the particular point of $U = \infty$ where all states with different spin are degenerate. For $t_2 = -0.2$ (and all other cases with one minimum in the single-particle spectrum) U_c increases monotonically with n. As $n \to 0$, $U_c \to 0$, which seems to imply that the problem could be treated perturbatively in this limit. However, the relevant parameter here is actually U_c divided by n which tends to a finite value rather than going to zero at small densities (see Fig. 10).

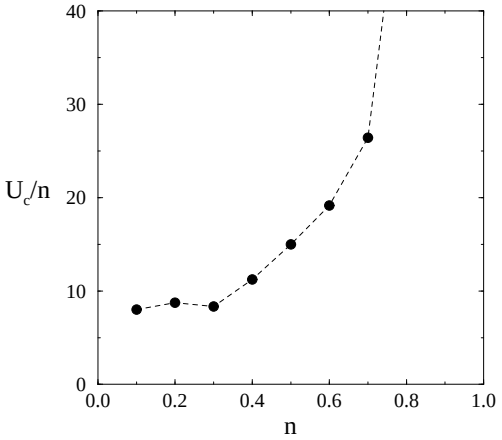

FIG. 10. Renormalized U_c as a function of density for $L = 50$ and $t_2 = -0.2$.

For the two cases $t_2 = -0.8$ and $t_2 = -2$, a local minimum appears near $n = 0.6$ and $n = 0.8$, respectively. This minimum in U_c is due to a diverging density of states at the Fermi energy of the fully polarized state. This occurs at a critical density n_c where the Fermi energy coincides with the local maximum in $\epsilon(k)$ at $k = 0$, which exists only for $|t_2| > 0.25$. For $t_2 = -2$ there exists a finite range of densities in which the system never becomes ferromagnetic, even at $U = \infty$. Nevertheless, around the critical density there still exists a finite U_c with a minimum value at n_c.

B. Luttinger liquid parameters

The Luttinger liquid concept[45] (for a review see Ref. 46 or Ref. 47) is based on a single-particle spectrum with two Fermi points ($\pm k_F$). This is the case in the $t_1 - t_2$ model for all densities when $|t_2| < 0.25$ and for large enough fillings when $t_2 < 0.25$ (see Fig. 2). The spectrum is linearized in the region of these two points and therefore completely specified by the Fermi velocity v_F.

The interaction between electrons can then be written in terms of four scattering processes: backward scattering (g_1), forward scattering (g_2), Umklapp scattering (g_3) connecting the region around $+k_F$ with that

around $-k_F$, and a g_4 term connecting states on the same branch, either around $+k_F$ or around $-k_F$. The g_4 term, which is usually neglected since it leads only to a renormalization of the Fermi velocity, will be seen to be important here.

We consider a non-half-filled system, where Umklapp process can be neglected. Using bosonization, the Hamiltonian can be written in terms of boson field operators ϕ_ν and their canonically conjugate fields Π_ν ($\nu = \rho, \sigma$ for charge and spin). This leads to the spin-charge separated Hamiltonian

$$H = H_\rho + H_\sigma + \frac{2g_1}{(2\pi\alpha)^2}\int dx \cos\left(\sqrt{8}\phi_\sigma\right). \qquad (22)$$

Here α is a short-distance cutoff of the order of the lattice spacing and

$$H_\nu = \int dx \left[\frac{\pi u_\nu K_\nu}{2}\Pi_\nu^2 + \frac{u_\nu}{2\pi K_\nu}\left(\partial_x\phi_\nu\right)^2\right] \qquad (23)$$

is the Hamiltonian of an elastic string with eigenmodes corresponding to the collective density fluctuations of the fermion liquid. The new parameters are the charge and spin velocities given by[47]

$$u_\sigma = \sqrt{{v_F}^2 - \left(\frac{g_1}{2\pi}\right)^2} \qquad (24)$$

$$u_\rho = \sqrt{\left(v_F + \frac{g_4}{\pi}\right)^2 - \left(\frac{g_1 - 2g_2}{2\pi}\right)^2} \qquad (25)$$

and the two coefficients K_ρ and K_σ which determine the asymptotic behavior of correlation functions ($K_\sigma = 1$ for the Hubbard model due to the SU(2) spin symmetry).

We can then calculate physical quantities such as the spin susceptibility

$$\chi = \frac{2}{\pi}\frac{K_\sigma}{u_\sigma} \qquad (26)$$

or the density-density correlation function

$$\langle \delta n(x)\delta n(0)\rangle = -\frac{K_\rho}{(\pi x)^2} + A_1\cos(2k_F x)\frac{1}{x^{1+K_\rho}\log^{3/2} x} + \cdots, \qquad (27)$$

where $\delta n(x) = n(x) - \langle n(x)\rangle$.

1. Determination of K_ρ

To obtain K_ρ using DMRG we compute the Fourier transform

$$C(q) = \frac{1}{\sqrt{L}}\sum_\ell e^{iq\ell} N_{\rm ave}(\ell) \qquad (28)$$

of the charge-charge correlation function (27) and then take the first derivative at $q = 0$

$$\left.\frac{\partial C(q)}{\partial q}\right|_{q=0} = \frac{K_\rho}{\pi}. \qquad (29)$$

The $q = 0$ derivative is proportional to the coefficient of the $1/x^2$ term in Eq. (27). This method of extracting K_ρ has been shown to yield accurate results for the exactly solvable case $t_2 = 0$ and should be valid as long as the system is in the Luttinger liquid phase.[48] Since we work with open boundary conditions we have to use zero padding for $|\ell| > L$ and average the correlation function to reduce boundary effects[49]:

$$N_{\rm ave}(\ell) = \frac{1}{n_a}\sum_{m=0}^{n_a-1} N(i_0+m, i_0+\ell+m) \qquad (30)$$

where $i_0 + \ell/2 = L/2$ and

$$N(i,j) = \langle n_i n_j\rangle - \langle n_i\rangle\langle n_j\rangle. \qquad (31)$$

The quantity n_a is taken to be large enough so that $N_{\rm ave}(\ell)$ does not depend strongly on i_0 and n_a; typically we take $n_a \approx 6$.

The correlation functions for a system of size $L = 100$ and $t_2 = -0.2$ with density $n = 0.5$ are given in Fig. 11. One can see that the slope at $q = 0$ is well-behaved and decreases monotonically with increasing U.

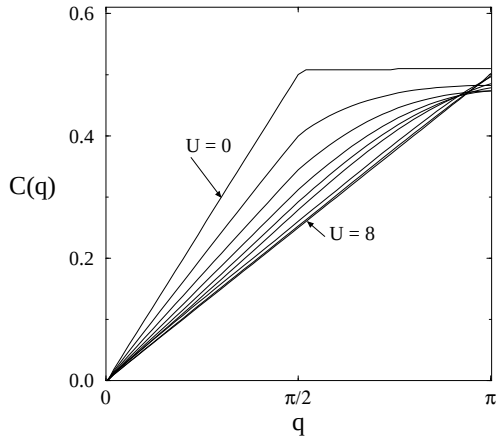

FIG. 11. Fourier transform $C(q)$ of the density-density correlation function for systems of size $L = 100$, $t_2 = -0.2$, $n = 0.5$ and $U = 0, 1, \ldots, 8$.

Therefore K_ρ can be accurately calculated using Eq. (29). In Fig. 12 the numerical results for $t_2 = -0.2$ are compared with the well-known values for the simple ($t_2 = 0$) Hubbard chain,[50] where the appropriate parameter in the weak-coupling regime is U/v_F. It is seen that the two curves agree very well for weak couplings, although the Fermi velocities differ appreciably: $v_F(t_2 = 0)/v_F(t_2 = -0.2) \approx 2.3$. The deviation between the two curves increases for larger couplings. For $t_2 = 0$, K_ρ goes asymptotically to the value $\frac{1}{2}$ as $U \to \infty$, whereas for $t_2 = -0.2$ K_ρ reaches $\frac{1}{2}$ at a finite U whose value agrees quite well with the U_c calculated above.

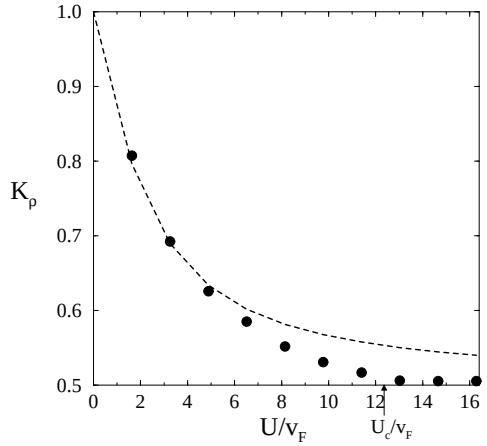

FIG. 12. K_ρ as function of U for $n = 0.5$. The filled circles are for $t_2 = -0.2$ and the dashed line is for $t_2 = 0$.

2. Spin and charge velocities

To determine the velocity of the spin and charge excitations, we use finite-size scaling of the corresponding energy gap

$$\Delta_\nu = u_\nu \Delta k = u_\nu \frac{\pi}{L+1} \tag{32}$$

where Δk is the finite interval between two adjacent k-points for open boundary conditions. The spin gap is defined as[51]

$$\Delta_\sigma = E_0(S=1) - E_0(S=0) \tag{33}$$

where $E_0(S)$ is the lowest eigenvalue for a system with spin S, and the charge gap is given by

$$\Delta_\rho = \frac{1}{2}\left[E_0(N+2) + E_0(N-2) - 2E_0(N)\right] \tag{34}$$

where $E_0(N)$ is the ground state energy for N particles and $S_z = 0$.

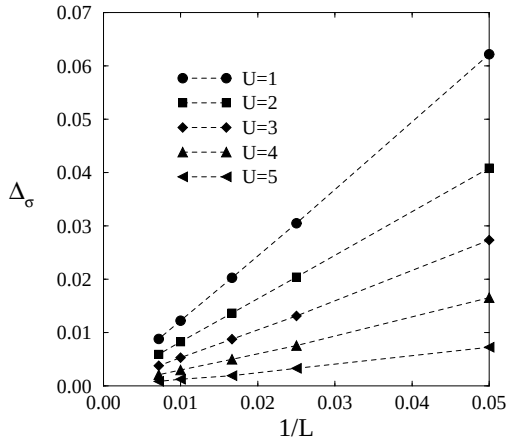

FIG. 13. Spin gap for different values of U for systems with $t_2 = -0.2$ and $n = 0.5$.

In Fig. 13, we show the finite-size scaling of the spin gap for a system with density $n = 0.5$ and $t_2 = -0.2$ for increasing values of U (from 1 to 5). For these parameters, $U_c \approx 7.55$. The excitations are gapless, as expected, and the spin velocity u_σ decreases to 0 with increasing U. Here $K_\sigma = 1$ due to the SU(2) invariance, and the susceptibility (26) is then directly proportional to u_σ^{-1}. Hence, as can be seen in Fig. 14, χ diverges when approaching U_c. A diverging susceptibility is an indication of a second-order transition, in accordance with the analysis of Sec. IV C. The critical exponent γ is defined near the transition by

$$\chi \sim u^{-\gamma}, \tag{35}$$

where $u = |U - U_c|$. We obtain $\gamma = 2.0 \pm 0.1$ by fitting the results shown in Fig. 14, where the error is from the least–squares fit.

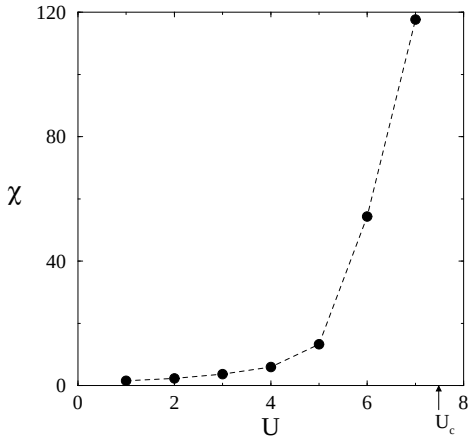

FIG. 14. Spin susceptibility as a function of U for a system with $t_2 = -0.2$ and $n = 0.5$.

We have also calculated the charge velocity. In Fig. 15 we show the results for the same parameters as above and compare them with the case $t_2 = 0$ (obtained following Ref. 50). We notice that for $t_2 = -0.2$ the charge velocity, u_ρ, is strongly renormalized from the $t_2 = 0$ value as U is increased, even when U is rescaled by the Fermi velocity. Eq.(25) suggests that this behavior could be governed by the g_4 term which describes scattering between states on the same branch of the spectrum and whose effect is usually taken to be unimportant. The increased importance of the g_4 interaction in a system with a tendency towards ferromagnetism is understandable since the system's response to an external magnetic field is described in terms of the operator

$$O = \sum_{k,\sigma} \sigma \left[c^\dagger_{(k_F+k)\sigma} c_{(k_F+k)\sigma} + c^\dagger_{(-k_F+k)\sigma} c_{(-k_F+k)\sigma} \right] \tag{36}$$

which involves states on the same branch of the spectrum. This indicates that g_4 must appear in the renormalization

of the corresponding response function. Hence the g_4 term must be relevant for the ferromagnetic fixed point, and we would therefore expect u_σ to be strongly rescaled.

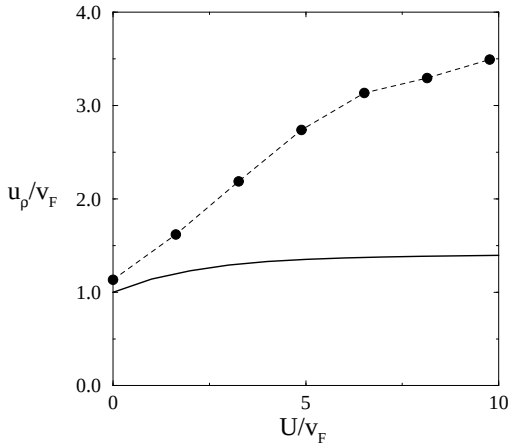

FIG. 15. The charge velocity u_ρ as a function of U for $t_2 = 0$ (full line) and $t_2 = -0.2$ (filled circles).

C. Spin-spin correlation function

We can also study the behavior of the spin-spin correlation function near the transition. In order to minimize effects of the open boundary conditions, we average over a number of sites for a given distance, as was done for the density-density correlation function in Sec. V B 1, and consider

$$S_{\rm ave}(\ell) = \frac{1}{n_a} \sum_{m=0}^{n_a-1} S(i_0+m, i_0+\ell+m), \qquad (37)$$

where $i_0 + \ell/2 = L/2$, $n_a \approx 4$ and

$$S(i,j) = \langle S_i^- S_j^+ \rangle. \qquad (38)$$

Fig. 16 shows the result for values of U near U_c. We find that $S_{\rm ave}(\ell)$ is positive definite, indicating ferromagnetic correlations, and can be well-fitted by the form $e^{-\ell/\xi}$, with ξ diverging as the transition is approached. This is seen by the linear behavior of $S_{\rm ave}(\ell)$ on the semi-log plot, with decreasing slope as U increases and the transition is approached. We can define the critical exponent associated with the divergence of the correlation length as

$$\xi \sim u^{-\nu} \qquad (39)$$

where $u = |U - U_c|$. Unfortunately, near the transition mixing of energetically close states make it numerically difficult to accurately calculate $S_{\rm ave}(\ell)$, even using 7 iterations and keeping up to 800 states. There tend to be systematic errors, which we minimize by limiting the system size to $L = 40$. However, ξ then quickly becomes of the order of the system size as the transition is approached, so that we can at most say that the best fit to the data occurs with a relatively small value of ν, $\nu \approx 0.2$.

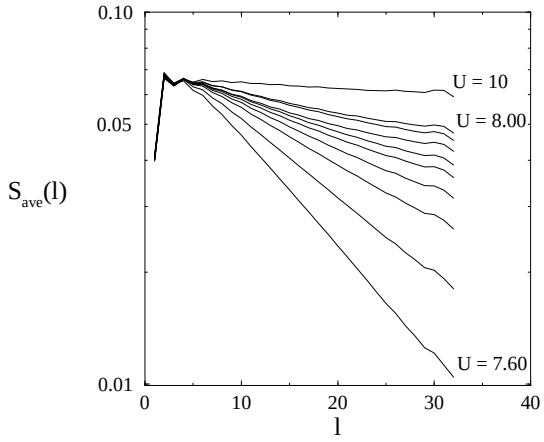

FIG. 16. The averaged spin-spin correlation function $S_{\rm ave}(\ell)$ for a system with $L = 40$, $t_2 = -0.2$ and $n = 0.5$ for $U = 7.60, 7.65, \ldots, 8.00$ and 10, plotted on a semilog scale.

The total spin S of the ground state is also related to this correlation function (see Eq. (14)) via

$$\langle \mathbf{S}^2 \rangle = S(S+1) = S_z(S_z+1) + \sum_{i,j} \langle S_i^- S_j^+ \rangle, \qquad (40)$$

which for a translationally invariant system becomes

$$S(S+1) = S_z(S_z+1) + L \sum_\ell S(\ell), \qquad (41)$$

where $S(\ell) = \langle S_i^- S_{i+\ell}^+ \rangle$ is independent of i. Therefore, the ferromagnetic order parameter is

$$s = S/L \sim L^{-1/2} \left[\sum_\ell S(\ell) \right]^{1/2}. \qquad (42)$$

If $\sum_\ell S(\ell)$ is finite for $L \to \infty$, the system is disordered; if it is proportional to L, there is long-range ferromagnetic order; and if it follows a power law $L^{2-\eta}$ with $1 < \eta < 2$, the system is at the critical point with critical exponent η and $S(\ell) \sim \ell^{1-\eta}$. In the ordered ferromagnetic phase, we do find a nonzero value of $S(\ell)$ at large distances as seen in Fig. 16, consistent with this picture, but we have not been able to determine the critical exponent η from numerical calculations because of the poor convergence of the DMRG at the critical point and because of uncertainty in U_c.

VI. PHASE DIAGRAM

A. $U = \infty$ phase diagram

The phase diagram for $U = \infty$ can be determined using DMRG calculations. While one could, in principle, start with a Hilbert space in which double occupancy is explicitly excluded, here we simply set $U = 10^6$ to mimic the infinite-U limit and find that the accuracy is quite good since the DMRG integrates out high energy scales automatically. In order to decide if a point in the $n - t_2$ plane is ferromagnetic or not, we compare its DMRG energy E_D with the known ferromagnetic energy $E_{\rm ferro}$ and, in addition, calculate $\langle \mathbf{S}^2 \rangle = S(S+1)$ and compare it with $S_{\rm max}$. If $S \approx S_{\rm max}$ and $E_D > E_{\rm ferro}$ for given t_2 and n we conclude that the system is ferromagnetic for these parameters, whereas if we find an energy E_D lower than $E_{\rm ferro}$ and $S \approx 0$, we conclude that it is non-magnetic. Near the boundary between these two regions we sometimes find partly polarized states, i.e. $E_D < E_{\rm ferro}$ but $S > 0$. It is difficult to determine the nature of these states because there are two possible causes for the partially polarized value of S. One possibility is that the system undergoes a continuous phase transition as a function of n or t_2 at $U = \infty$. However, near a ferromagnetic phase transition, near-degeneracy of states leads to a mixing of states in the diagonalization step of the DMRG procedure. Therefore, the presence of partially polarized states could also be due to numerical effects. This mixing can also be seen in that the values of S obtained in general take on continuous values that lie between the discrete values of S allowed by the finite number of electrons in the system. These problems are similar to those that occur near the ferromagnetic transition at finite U discussed in Sec. IV C, where we used extremely accurate exact diagonalization calculations instead of DMRG to solve them.

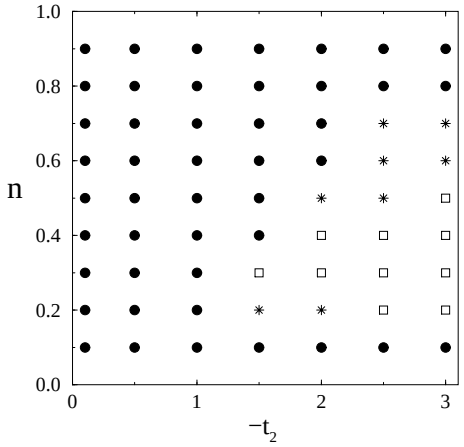

FIG. 17. Phase diagram for $U = \infty$ and $L = 30$ obtained with DMRG. The filled circles indicate a fully polarized ground state, the open square a non-magnetic ground state and the stars a partially polarized ground state.

As seen in Fig. 17, we obtain a large region of ferromagnetism. The three limiting cases of Sec. II C are reproduced and the corresponding ferromagnetic regions are, in fact, connected. We also notice that for sufficiently large $|t_2|$, the system is not magnetic at intermediate densities. This extends the limit $t_2 \to -\infty$ in which the system consists of two uncoupled Hubbard chains which must be non-magnetic due to the Lieb-Mattis theorem,[10] to a finite region. In this region, the system behaves effectively like an uncoupled two-chain model. We will later present evidence that this region in which the system behaves as two uncoupled Hubbard chains extends to the low-U phase diagram. Note that this phase diagram is qualitatively similar to that obtained using the Edwards ansatz (see Fig. 5), except that here the entire t_2 axis is ferromagnetic for small densities.

B. Low-U phase diagram

We now turn to the general question of the low U phase diagram within a weak-coupling analysis. Balents and Fisher[32] have analyzed the weak-coupling phase diagram of the two-chain Hubbard model using RG and bosonization. Their calculation is generic for a system with four Fermi points. They obtain coupled RG equations and integrate them numerically to find the different fixed points, which they then analyze using bosonization. The possible phases can be classified by the number of charge and spin modes which are gapless. A phase with α gapless charge modes and β gapless spin modes is denoted CαSβ, where α and β can take on integer values from 0 to 2. An adaption of their two-chain phase diagram to the t_1-t_2 model in the t_2-n plane is shown in Fig. 18, with the $t_2 < 0$, $n < 1$ quadrant shown in more detail in Fig. 19.

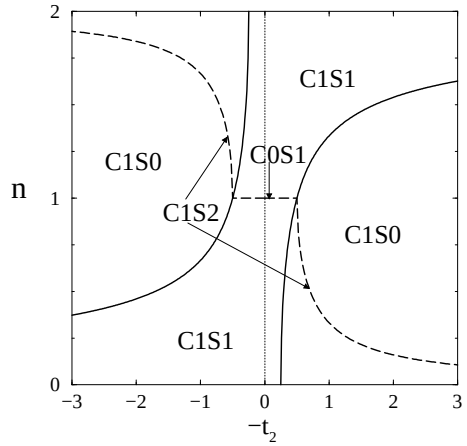

FIG. 18. Low-U phase diagram obtained by adapting the results of Ref. 32. Some small regions of additional phases near the solid lines are not shown.

As discussed in Sec. V B, a Luttinger liquid phase (C1S1) is expected for small $|t_2|$ in the region where

the $U = 0$ system has two Fermi points. At half-filling $2k_F = \pi$ and umklapp processes cause the system to open a charge gap, so that the phase is that of the one-dimensional Heisenberg model (C0S1).

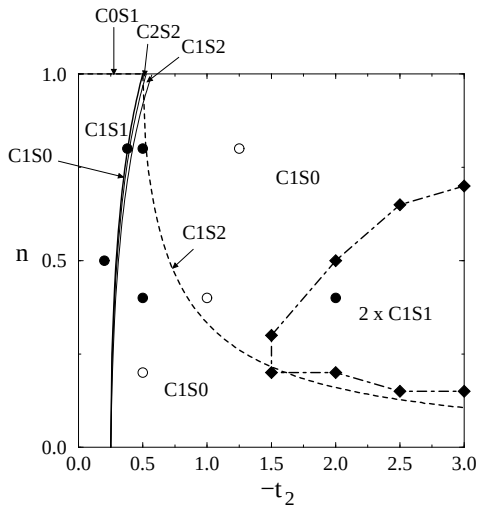

FIG. 19. Low-U phase diagram restricted to negative t_2 and $n < 1$. The filled circles are for parameters for which no spin gap has been found with DMRG at $U = 2$, while the open circles are for parameters where a spin gap has been found.

When the Fermi surface has four points, namely $\pm k_{F_1}$ and $\pm k_{F_2}$, the effective low-energy model has four linearized single-particle branches $\epsilon_1(k) = \mp v_{F_1}(k - k_{F_1})$ and $\epsilon_2(k) = \pm v_{F_2}(k - k_{F_2})$ (see Fig. 20).

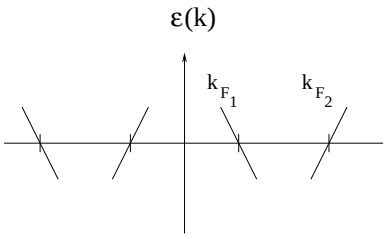

FIG. 20. Effective low-energy model for a Fermi surface with four points.

This is equivalent to the two-band model of Ref. 32 for which there are also four Fermi points, namely $\pm k_F^b$ for the bonding, and $\pm k_F^a$ for the antibonding band. The only difference here is that the inner bands, which are denoted $\epsilon_1(k)$ in the present case and originate from the antibonding band in the two-chain model, have opposite velocities. The correct mapping of the Fermi points between the two models is therefore

$$\pm k_{F_1} \to \mp k_F^a$$
$$\pm k_{F_2} \to \pm k_F^b.$$

Provided that this mapping is performed, the perturbation expansion of the $t_1 - t_2$ model and the two-chain Hubbard model is exactly the same at low energy, as already pointed out by Fabrizio.[30] Therefore, we can simply adapt the results from Ref. 32 to our case. In Fig. 18 and Fig. 19, the thick solid line represents the critical density n_c for which the Fermi surface splits into four points (cf. Fig. 2). Exactly on this line, Balents and Fisher predict a C1S0 phase. For slightly smaller densities, v_{F_1} is much smaller than v_{F_2} leading first to a C2S2, then to a C1S2 phase. (These three phases are not depicted in Fig. 18 since they have a small extent.) When v_{F_1} is comparable to v_{F_2} the weak-coupling RG leads to a large region of a C1S0 phase. This phase is a doped spin-liquid phase with a spin gap in which power-law pairing and CDW correlations coexist.[53] When $2k_{F_2} = \pi$ within this region, indicated by a dashed line, umklapp processes in the corresponding bonding band can open a charge gap. For the two-chain model, Balents and Fisher predict a C1S2 phase along some of this line, with the result being sensitive to the initial conditions in the RG equations, i.e. on v_F and the initial couplings.

In order to investigate the validity of this weak-coupling phase diagram, we have calculated the spin and charge gaps using the DMRG for different system sizes at small U (we choose $U = 2$) and a number of t_2 and n values. Due to the weak coupling and small size of the gaps, very high precision is necessary in the DMRG procedure. We use up to 8 finite-size iterations and keep up to 800 states in the last iteration. The presence of a spin gap in the extrapolated $L \to \infty$ limit is indicated by an open circle in Fig. 19 and the absence of a spin gap by a solid circle.

Figs. 21 and 22 show the finite-size scaling of the charge and spin gap. The filled circles represent the spin gap and the open squares the charge gap while the lines are quadratic regression in $(\frac{1}{L})$ between the points. In general, the finite-size corrections to the spin and charge gaps for a system with open boundaries can be represented as a power series in $1/L$. When a gap is present, the dominant correction is usually $1/L^2$, and when the system is gapless, the dominant correction[54] is $1/L$. While this behavior is generally seen in Figs. 21 and 22, there are cases with a small gap with an obvious positive quadratic correction, but also a substantial linear term. In addition, there is scatter of up to the order of the symbol size in some of the curves which we believe is due to additional finite-size effects which can oscillate with the number of particles.

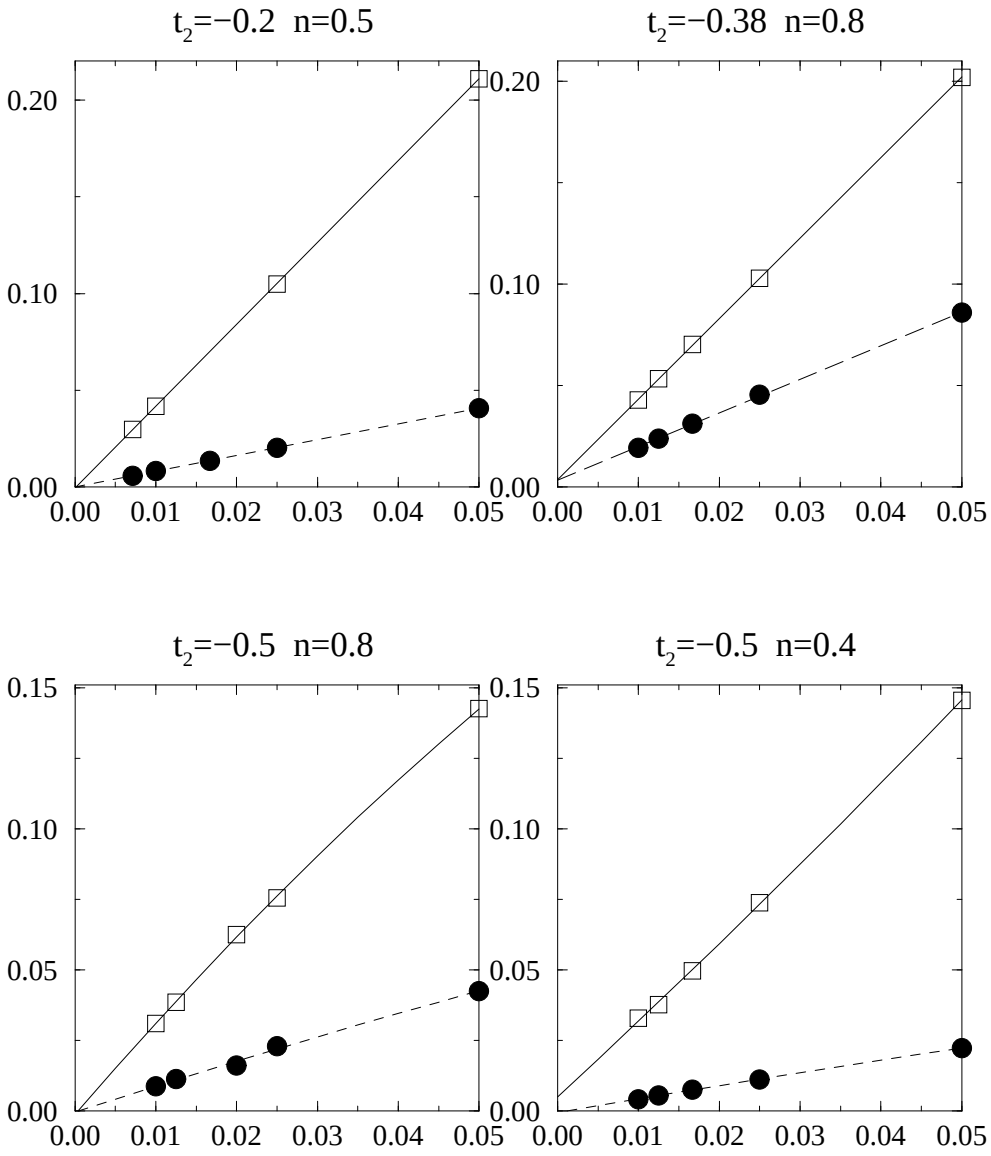

FIG. 21. Finite-size scaling of charge (open squares) and spin (filled circles) gap for different parameters.

For $t_2 = -0.2, n = 0.5$, the clearly vanishing charge and spin gaps confirm that the system behaves as a Luttinger liquid (see Sec. V B). For parameters close to the line of critical n, namely $t_2 = -0.5, n = 0.4$ and $t_2 = -0.5, n = 0.8$, we find no spin and charge gap, in contradiction with the adapted weak-coupling phase diagram. However, a finite U could renormalize the band structure, leading to a shifting of the line of transition from two Fermi points to four. Such a shift is seen with increasing U in the two-chain Hubbard model.[55] Precisely on this transition line, for $t_2 = -0.38, n = 0.8$, a spin gap would be predicted, but we do not find one. However, this phase might be hard to see numerically since it occurs only exactly on the line, or might not be present for finite U. Such a phase has also not been found numerically in the two-chain Hubbard model.[49]

For the case $t_2 = -1.25, n = 0.8$ we find a spin gap, as predicted. For $t_2 = -0.5, n = 0.2$, where a spin gap is also predicted, we have taken $U = 0.5$ rather than $U = 2$ because the ground state is not paramagnetic at the larger U value due to the proximity of the ferromagnetic transition. At the smaller U, finite size effects and numerical problems make it difficult to definitely determine whether or not there is a spin gap. Nevertheless, since there is a strong quadratic correction, we conclude that a spin gap is probably present.

Near the line $2k_{F_2} = \pi$, (i.e. at $t_2 = -1, n = 0.4$) the system has a small spin gap, consistent with the C1S0 phase but not a possible C1S2 phase. However, as pointed out above, the existence of the C1S2 phase in the weak–coupling

calculation is dependent on the initial conditions, so it may not be present along all of the dashed line. In the two-chain Hubbard model, numerical DMRG calculations[49] do find evidence for this phase for some fillings, even at intermediate to strong U. More work would have to be done to determine in detail some of the finer structure of the phase diagram, but the difficulty of the calculations and the finite-size scaling preclude a more detailed investigation here.

For $t_2 = -2.0$ and $n = 0.4$, we find that both the spin and the charge gaps vanish, in contradiction to the weak-coupling phase diagram, which would predict a C1S0 phase. This occurs in the regime which is paramagnetic at large U because the system behaves as two uncoupled chains (see Sec. VI A). We therefore suspect that the strong-coupling behavior extends to weak coupling, and that the system is in a $2 \times$ C1S1 = C2S2 phase here. The phase boundary of the paramagnetic strong-coupling phase, indicated by the solid diamonds, is also sketched in. It remains to be determined how much this phase boundary changes in going from strong to weak U.

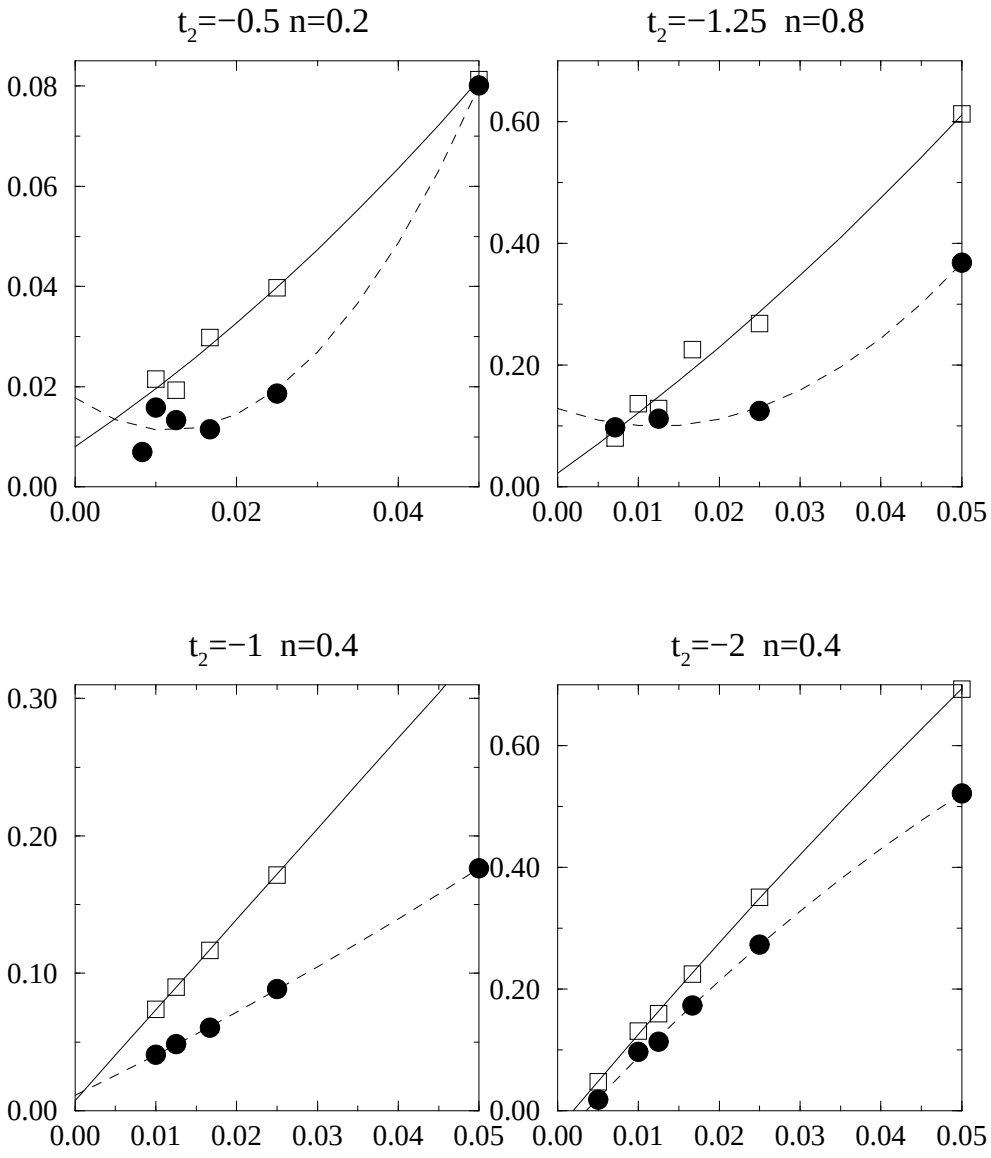

FIG. 22. Finite-size scaling of charge (open squares) and spin (filled circles) gap for different parameters.

It should also be noted that Kuroki et al.[31] have studied the t_1-t_2 model numerically using Projector Quantum Monte Carlo and the DMRG at half-filling and $t_2 = -0.8$ and find a spin-gapped metallic phase with dominant pairing correlations at weak U, in agreement with Fig. 18 and Ref. 30. As U is increased they find a transition to a spin-gapped insulating phase also in agreement with Ref. 30. Here we have concentrated on $n < 1$ in the numerical work since the ferromagnetic phase is not present at $n = 1$. In very recent work that we became aware of as this manuscript was being completed, Arita et al.[56], have calculated the spin gap at $n = 1.0$ and $n = 0.5$ and $t_2 = -0.55, -0.8, -2.0$ using the DMRG. Of particular interest for the weak-coupling phase diagram are the $n = 0.5$, $t_2 = -0.8, -2.0$ points which are in a paramagnetic phase. For the $t_2 = -0.8$ point, they find a very small but finite gap at $U = 8$, consistent with a C1S0 phase. However, we believe that their data are also consistent with a vanishing spin gap, which would be consistent with the C1S2 phase present along the dashed line in Fig. 19. At $t_2 = -2.0$ and $U = 16$, they find a vanishing spin gap, in contradiction with the weak-coupling prediction of a gapped C1S0 phase at these parameters, but consistent with the $2 \times$ C1S1 phase proposed above.

VII. CONCLUSION

We have studied an extended version of the conventional one-dimensional Hubbard model in order to investigate the mechanism for ferromagnetism in an itinerant electron model. The added term, which involves hopping between next-nearest neighbor sites, precludes the application of the Lieb-Mattis theorem[10] which excludes a ferromagnetic ground state in the one-dimensional Hubbard model. Indeed, we do find a ferromagnetic phase in a wide region of parameters at large enough U in the regime with t_2 negative and $n < 1$ (which is equivalent to the $t_2 > 0$, $n > 1$ region through a particle-hole transformation).

Using exact diagonalization, the Density-Matrix Renormalization Group and the Edwards variational ansatz, we have shown that the three different mechanisms for ferromagnetism obtained by taking special limits at $U = \infty$ (the Nagaoka state, the limit of vanishing density and the limit of very small t_2) are all connected in the same phase in the t_2–n plane. For large negative t_2/t_1, there is a paramagnetic region in the large–U phase diagram in which the system behaves like two independent Hubbard chains. This region extends to $t_2 \approx -1.5$ at intermediate n.

The critical interaction strength for the ferromagnetic transition, U_c, has three characteristic behaviors as a function of n. When $0 > t_2 > -0.25$, there is one minimum in the single-particle dispersion, $\epsilon(k)$, and U_c increases monotonically with n. For $-0.25 > |t_2| > -1.5$, there are two minima in $\epsilon(k)$, and there is a local minimum in U_c when the Fermi level of the fully polarized ferromagnetic state is at the singularity in the density of states corresponding to the local maximum in $\epsilon(k)$. Finally, when $|t_2| < -1.5$, there is an intermediate region on n for which there is no ferromagnetism, even at $U = \infty$, but there is a finite local minimum in U_c when the Fermi energy is at the local maximum in $\epsilon(k)$.

This leads us to the question of what general properties are required in order to obtain metallic ferromagnetism in this model. The general picture is that with hole doping, t_2 must be less than zero in order to obtain a ferromagnetic state. When this condition is satisfied, the ferromagnetic state occurs over a wide range of parameters, with, in some cases, quite small U_c. The mechanism for ferromagnetism can be motivated from a local point of view, in that when t_2 is negative the triangular structure of the chain frustrates the antiferromagnetic order (a generic effect for lattice models). That this frustration can lead to a ferromagnetic ground state can be seen on small cluster calculations.

Another point of view emphasizes the importance of the form of the single-particle density of states. Wahle et al.,[57] for example, emphasize that a necessary condition for ferromagnetism is an asymmetric density of states, with a strong singularity and a larger density of states in the lower part of the band. Our results here also support these ideas. For $t_2 = 0$, the density of states is symmetric and there is no ferromagnetism. When $t_2 < 0$ the density of states becomes asymmetric, with the $\epsilon^{-1/2}$ Van Hove singularity at the lower band edge gaining in weight. For $t_2 < -0.25$, the presence of the additional Van Hove singularity at the ferromagnetic Fermi level further stabilizes the ferromagnetic ground state.

The weak-coupling behavior of this model has also proven to be quite interesting. For weak negative t_2, the low-energy effective behavior of the model does not differ qualitatively from that of the one-dimensional Hubbard model. For weak U, we do indeed find that the model is well-described as a Luttinger liquid, and have been able to extract the Luttinger-liquid parameters, K_ρ, u_ρ and u_σ using the DMRG. However, unlike the one-dimensional Hubbard model, the Luttinger liquid state of the t_1-t_2 model undergoes a transition to a ferromagnetic state at finite U. While it is clear that the breakdown of the Luttinger liquid is not described within the usual weak-coupling picture, we have tried to indicate how the breakdown occurs within this picture. The spin velocity, which goes to zero asymptotically as $U \to \infty$ in the $t_2 = 0$ case, becomes zero at finite U_c for $t_2 < 0$. The ferromagnetic susceptibility, which is inversely proportional to the spin velocity in a Luttinger liquid thus diverges at the transition, implying that the transition is second order. By fitting this susceptibility with the form $|U - U_c|^{-\gamma}$, we obtain a critical exponent $\gamma = 2.0 \pm 0.1$.

In addition, we have calculated the spin-spin correlation function in the vicinity of the transition and find that it becomes ferromagnetic and exponentially decaying just below the transition. The correlation length grows as the

transition is approached from below, which is consistent with a second order transition. We have attempted to extract a critical exponent ν by fitting the correlation length to a form $\xi \sim |U - U_c|^{-\nu}$, but find that it is difficult to extract an exponent due to convergence problems which limit the maximum lattice size near the transition.

An examination of the behavior of the ground state energy as function of U near the transition using exact diagonalization suggests that $E_0(U)$ becomes smooth in the thermodynamic limit and provides further evidence that the transition is second order.

Finally, we have investigated the very rich low-U phase diagram. For a large region of parameters the low-U phase diagram of the t_1-t_2 model can be mapped to that of the two-chain Hubbard model. For sufficiently large $|t_2|$ and a wide range of $n < 1$, we confirm numerically the existence of the doped spin-liquid phase (C1S0) predicted by weak coupling RG, which is the one-dimensional analog of a superconducting phase. In addition, we have presented evidence for the existence of a new $2 \times$ C1S1 phase (not found in the weak coupling treatment) in a region in which we think that the $t_1 - t_2$ model behaves as two uncoupled Hubbard chains. Because we have also found some additional discrepancies between the weak-coupling phase diagram and the numerical calculations, more work needs to be done to clarify the details of the phase diagram for the lattice model.

ACKNOWLEDGMENTS

This work was supported by the Swiss National Foundation under the Grant No. 20-46918.96. We would like to thank D. Baeriswyl, M. Dzierazawa, and J. Voit for helpful discussions.

VIII. TABLES

C_{4v}	E	$2C_4$	C_2	$2\sigma_v$	$2\sigma_d$
A_1	1	1	1	1	1
A_2	1	1	1	−1	−1
B_1	1	−1	1	1	−1
B_2	1	−1	1	−1	1
E	2	0	−2	0	0

TABLE I. Character table of the group C_{4v}.

A_1 :	$-2t_2 + \sqrt{4t_2^2 + 8t_1^2}$	E :	$-2t_1$
	$-2t_2 - \sqrt{4t_2^2 + 8t_1^2}$		$-2t_1$
A_2 :	$4t_2$		0
B_1 :	$4t_2$		0
B_2 :	$-4t_2$		$2t_1$
	0		$2t_1$

TABLE II. Eigenvalues of the square model for $N = 2$.

A_1 :	$t_1 - 2t_2$	E :	$-2t_2$
A_2 :	$-2t_1 + 2t_2$		$-2t_2$
	$t_1 + 2t_2$		$-\sqrt{3t_1^2 + 4t_2^2}$
B_1 :	$2t_1 + 2t_2$		$-\sqrt{3t_1^2 + 4t_2^2}$
	$-t_1 + 2t_2$		$\sqrt{3t_1^2 + 4t_2^2}$
B_2 :	$-t_1 - 2t_2$		$\sqrt{3t_1^2 + 4t_2^2}$

TABLE III. Eigenvalues of the square model for $N = 3$.

APPENDIX A: EDWARDS ANSATZ

The gradient of E with respect to the one-particle orbitals $\varphi_\alpha(j) = \varphi_{\alpha j}$ can for real wave functions be simplified to

$$\frac{\partial E}{\partial \varphi_{\alpha j}} = 2\langle\chi|(H-E)\frac{\partial}{\partial \varphi_{\alpha j}}|\chi\rangle. \tag{A1}$$

This expression can be evaluated using Wick's theorem, yielding

$$\frac{\partial E}{\partial \varphi_{\alpha j}} = F^{\downarrow}_{\alpha j} + F^{\uparrow}_{\alpha j} + F^{U}_{\alpha j} \tag{A2}$$

where

$$\begin{aligned}
F^{\downarrow}_{\alpha j} &= -t_1\cos(q)\det S^{(1)}\left\{\sum_\beta \varphi_{\beta j+1}[{S^{(1)}}^{-1}]_{\beta\alpha} + \varphi_{\beta j-1}[{S^{(1)}}^{-1}]_{\alpha\beta} - 2\varphi_{\alpha j}\right\} \\
&\quad -t_2\cos(2q)\det S^{(2)}\left\{\sum_\beta \varphi_{\beta j+2}[{S^{(2)}}^{-1}]_{\beta\alpha} + \varphi_{\beta j-2}[{S^{(2)}}^{-1}]_{\alpha\beta} - 2\varphi_{\alpha j}\right\} \\
F^{\uparrow}_{\alpha j} &= -t_1\cos(q)\left\{\sum_\beta \varphi_{\beta j}\left(S^{(1)}_{\alpha\beta} + S^{(1)}_{\alpha\beta}\right) - \varphi_{\alpha j+1} - \varphi_{\alpha j-1}\right\} \\
&\quad -t_2\cos(2q)\left\{\sum_\beta \varphi_{\beta j}\left(S^{(2)}_{\alpha\beta} + S^{(2)}_{\alpha\beta}\right) - \varphi_{\alpha j+2} - \varphi_{\alpha j-2}\right\} \\
F^{U}_{\alpha j} &= U\varphi_{\alpha 0}\left\{\delta_{j0} - \sum_\beta \varphi_{\beta 0}\varphi_{\beta j}\right\}
\end{aligned}$$

with overlap matrices $S^{(i)}_{\alpha\beta}$ defined as

$$S^{(i)}_{\alpha\beta} = \sum_{\ell=1}^{L} \varphi^*_\alpha(\ell)\varphi_\beta(\ell+i). \tag{A3}$$

[1] M. C. Gutzwiller, Phys. Rev. Lett. **10**, 159 (1963).
[2] J. Hubbard, Proc. Roy. Soc. A**276**, 238 (1963).
[3] J. Kanamori, Prog. Theor. Phys. **30**, 275 (1963).
[4] Y. Nagaoka, Phys. Rev. **147**, 392 (1966).
[5] P. Wurth, G. Uhrig and E. Müller-Hartmann, Ann. Physik **5**, 148 (1996).
[6] R. Hirsch, Dissertation (Universität Köln, 1994): *Zum Magnetismus stark korrelierter Fermionsysteme* (Verlag Shaker, Aachen 1994).
[7] S. Liang and H. Pang, Europhys. Lett. **32**, 173 (1995).
[8] P. Fazekas, B. Menge and E. Müller-Hartmann, Z. Phys. B **78**, 69 (1990).
[9] E. Lieb, Phys. Rev. Lett. **62**, 1201 (1989).
[10] E. Lieb and D. Mattis, Phys. Rev. **125**, 164 (1962).
[11] R. Strack and D. Vollhardt, Phys. Rev. Lett. **72**, 3425 (1994).
[12] M. Kollar, R. Strack and D. Vollhardt, Phys. Rev. B **53**, 9225 (1996).
[13] T. Okabe, to appear in Prog. Theor. Phys., preprint cond-mat/9707032.
[14] M. Fleck, A. M. Oles and L. Hedin, preprint (1996).
[15] J. Bünnemann, W. Weber and F. Gebhard, preprint.
[16] A. Mielke, Phys. Lett. A **174**, 443 (1993).
[17] A. Mielke and H. Tasaki, Commun. Math. Phys. **158**, 31 (1993).
[18] H. Tasaki, Phys. Rev. Lett. **25**, 4678 (1995).
[19] K. Penc, H. Shiba, F. Mila, T. Tsukagoshi and Phys. Rev. B **54**, 4056 (1996).
[20] M. Ulmke, preprint cond-mat/9704229.
[21] T. Hanisch, G. S. Uhrig and E. Müller-Hartmann, preprint cond-mat/9707286.
[22] T. Hermann and W. Nolting, preprint cond-mat/9702022.
[23] T. Obermeier, T. Pruschke and J. Keller, preprint cond-mat/9708156.
[24] P. Pieri, S. Daul, D. Baeriswyl, M. Dzierzawa and P. Fazekas, Phys. Rev. B **54** (1996).
[25] R. Hlubina, S. Sorella and F. Guinea, Phys. Rev. Lett. **78**, 1343 (1997).
[26] J. V. Alvarez, J. Gonzales, F. Guinea and M. A. H. Vozmediano, preprint cond-mat/9705165.
[27] Most results of this paper have been obtained in the framework of the Ph. D. thesis of S. Daul, Fribourg 1998, unpublished.
[28] S. Daul, P. Pieri, D. Baeriswyl, M. Dzierzawa and P. Fazekas, Physica B **230-232**, 1021 (1997).
[29] S. Daul and R. M. Noack, Z. Phys. B **103**, 293 (1997).
[30] M. Fabrizio, Phys. Rev. B **54**, 10054 (1996).
[31] K. Kuroki, R. Arita and H. Aoki, preprint cond-mat/9702214.
[32] L. Balents and M. P. A. Fisher, Phys. Rev. B **53**, 12 133 (1996).
[33] H. Tasaki, preprint cond-mat/9512169.
[34] P. W. Atkins, M. S. Child and C. S. G. Phillips, *Tables for Group Theory*, Oxford University Press (1970).
[35] D. C. Mattis and R. E. Peña, Phys. Rev. B **10**, 1006 (1974).
[36] M. Sigrist, H. Tsunetsugu, K. Ueda and T. M. Rice, Phys. Rev. B **46**, 13838 (1992).
[37] E. Müller-Hartmann, J. Low Temp. Phys. **99**, 349 (1995).
[38] D. M. Edwards, Prog. Theor. Phys. Suppl. **101**, 453 (1990).
[39] W. von der Linden and D. M. Edwards, J. Phys. : Condens. Matter 3, 4917 (1991).
[40] W. H. Preuss, S. A. Teukolsky, W. T. Vetterling and B. P. Flannery, *Numerical Recipes* (Cambridge University Press, 1995).
[41] C. Lanczos, Proc. Nat. Acad. Sci **20**, 529 (1934).
[42] E. R. Davidson, J. Computational Phys. **17**, 87 (1975).
[43] S. R. White, Phys. Rev. Lett. **69**, 2863 (1992); Phys. Rev. B **48**, 10345 (1993).
[44] S. R. White, Phys. Rev. Lett. **77**, 3633 (1996).
[45] F. D. M. Haldane, J. Phys. C **14**, 2585 (1981).
[46] J. Voit, Rep. Prog. Phys. **57**, 977 (1994).
[47] H. J. Schulz, Int. J. Mod. Phys. B bf 5, 57 (1991).
[48] M. Dzierzawa, in *The Hubbard model* , Ed. by D. Baeriswyl et al., New York (1995); S. Kneer, *Diploma Thesis*, Universität Würzburg, 1997.
[49] R. M. Noack, S. R. White and D. J. Scalapino, Physica C **270**, 281 (1996).
[50] H. Frahm and V. E. Korepin, Phys. Rev. B **42**, 10553 (1990).
[51] There are other definitions which actually converge better with L to the $L = \infty$ result. Indeed, for $t_2 = 0$ Bethe Ansatz calculations[52] show that $E_1(S_z = 1) - E_0(S_z = 1)$, where E_1 is the first spin-particle-hole-excitation, converges much faster with system size than Eq. (33).
[52] G. Bedürftig, private communication.
[53] For a discussion of the mechanism for pairing and the existence of a doped spin-liquid state in even-leg ladder materials, see E. Dagotto and T.M. Rice, Science, **271**, 618 (1996) and references therein.
[54] That the leading finite-size corrections to the spin gap for systems with open boundary conditions are $O(1/L^2)$ can be seen, for example, for Heisenberg ladders in S. R. White, R. M. Noack and D. J. Scalapino, Phys. Rev. Lett. **73**, 886 (1994).
[55] R. M. Noack, N. Bulut, D. J. Scalapino and M. G. Zacher, Phys. Rev. B **56**, 7162 (1997).
[56] R. Arita, K. Kuroki, H. Aoki and M. Fabrizio, preprint cond-mat/9712134.
[57] J. Wahle, N. Blümer, J. Schlipf, K. Held and D. Vollhardt, preprint cond-mat/9711242.